J. Fluid Mech. (2007), *vol.* 593, *pp.* 297–313.
doi:10.1017/S0022112007008786 Printed in the United Kingdom

Reflecting tidal wave beams and local generation of solitary waves in the ocean thermocline

T. R. AKYLAS[1], R. H. J. GRIMSHAW[2], S. R. CLARKE[3] AND ALI TABAEI[1]

[1]Department of Mechanical Engineering, Massachusetts Institute of Technology, Cambridge, MA 02139, USA

[2]Department of Mathematical Sciences, Loughborough University, Leics LE11 3TU, UK

[3]School of Mathematical Sciences, Monash University, Victoria 3800, Australia

(Received 1 December 2006 and in revised form 23 August 2007)

It is generally accepted that ocean internal solitary waves can arise from the interaction of the barotropic tide with the continental shelf, which generates an internal tide that in turn steepens and forms solitary waves as it propagates shorewards. Some field observations, however, reveal large-amplitude internal solitary waves in deep water, hundreds of kilometres away from the continental shelf, suggesting an alternative generation mechanism: tidal flow over steep topography forces a propagating beam of internal tidal wave energy which impacts the thermocline at a considerable distance from the forcing site and gives rise to internal solitary waves there. Motivated by this possibility, a simple nonlinear long-wave model is proposed for the interaction of a tidal wave beam with the thermocline and the ensuing local generation of solitary waves. The thermocline is modelled as a density jump across the interface of a shallow homogeneous fluid layer on top of a deep uniformly stratified fluid, and a finite-amplitude propagating internal wave beam of tidal frequency in the lower fluid is assumed to be incident and reflected at the interface. The induced weakly nonlinear long-wave disturbance on the interface is governed in the far field by an integral–differential equation which accounts for nonlinear and dispersive effects as well as energy loss owing to radiation into the lower fluid. Depending on the strength of the thermocline and the intensity of the incident beam, nonlinear wave steepening can overcome radiation damping so a series of solitary waves may arise in the thermocline. Sample numerical solutions of the governing evolution equation suggest that this mechanism is quite robust for typical oceanic conditions.

1. Introduction

Internal solitary waves are commonly observed in the coastal oceans and are often modelled by evolution equations of the Korteweg–de Vries type, appropriate for shallow waters (see, for instance, Grimshaw 2001; Helfrich & Melville 2006). In coastal regions it is generally accepted that these can be generated through the interaction of the barotropic tide with the continental shelf, generating an internal tide that in turn steepens and forms internal solitary waves as it propagates shorewards.

However, based on field observations in the Bay of Biscay, New & Pingree (1990) first suggested that ocean internal solitary waves may also arise from the interaction of a propagating internal tidal beam with the thermocline. In this alternative mechanism, the internal tidal beam is itself generated by tidal flow over steep topography near the

shelf break, but impacts the thermocline at a considerable distance from the forcing site and thereby generates internal solitary waves propagating offshore in deep water.

The field data in the Bay of Biscay revealed large-amplitude solitary wave packets about 150 km away from the shelf break. New & Pingree (1990, 1992) argued that it was unlikely for these waves to have travelled this far along the thermocline without experiencing significant dissipation. They conjectured that the observed solitary waves were instead generated locally by a propagating beam of internal tidal energy which had originated at the topography and, after reflecting from the bottom, encountered the thermocline close to the position where the solitary waves were found.

There are additional observations in the Bay of Biscay that support the hypothesis of a local generation mechanism. By analysing remote-sensing synthetic aperture radar data, New & da Silva (2002) identified packets of solitary waves in the vicinity of the shelf break as well as at a considerable distance (150–180 km) from the nearest topography; the latter were generated locally by a tidal wave beam originating from the shelf break, as both sets of solitary waves were seen to decay over 90–120 km of travel. Moreover, although earlier observations had focused on the northern and central parts of the Bay of Biscay, Azevedo, da Silva & New (2006) presented evidence from satellite images that the southern part of this bay is also a site with high-level internal solitary-wave activity, and the same local generation mechanism is applicable there as well.

On the theoretical side, Gerkema (2001) studied the local generation of solitary waves by internal tides in a two-layer flow configuration, representing the thermocline as a density jump across the interface of a relatively shallow homogeneous fluid layer on top of a finite-depth stratified fluid. The bottom topography had a smooth shelf profile, and a time-harmonic current of tidal frequency was used as forcing. Gerkema (2001) computed the linear hydrostatic response as an expansion in terms of the long-wave modes of this two-fluid system, and argued that local generation of solitary waves is the result of a two-stage process: an internal tidal beam originating at the topography first hits the thermocline and, via an essentially linear mechanism, excites an appreciable long-wave disturbance there, only if the thermocline is moderately strong – a condition that apparently was met in the Bay of Biscay according to the field data. Then, in the course of propagating along the thermocline, the disturbance triggered by the beam experiences the effects of dispersion and nonlinearity, thereby forming solitary waves. This scenario is supported by numerical simulations using a coupled equation system that allows for dispersive and nonlinear effects in the modal expansion of the response; the solitary waves gradually decay though, owing to leakage of energy in the lower fluid as they propagate along the thermocline.

In the present study, the thermocline again is modelled as a density jump across the interface of a homogeneous layer lying on top of a stratified fluid. However, attention is focused on the reflection of a tidal beam that is incident at the interface from the lower fluid, assumed to be infinitely deep, as well as on the evolution of the resulting interfacial disturbance, ignoring the process by which the beam is generated. A similar two-layer model was used by Thorpe (1998) to study nonlinear effects in the reflection of internal waves at the base of the ocean mixed layer. The approach taken here accounts for the essential ingredients of the mechanism for local generation of solitary waves, while avoiding a modal expansion. This makes it possible to derive a long-wave asymptotic model via suitable scaling of the governing equations, and thereby examine systematically the conditions under which solitary waves can arise.

Internal wave beams derive from the anisotropic nature of wave propagation in stratified fluids, since gravity provides a preferred direction. Ocean internal wave

beams, in particular, are excited by tidal flow over bottom topography as demonstrated by theoretical models (Bell 1975; Khatiwala 2003; Lamb 2004) as well as field measurements. In the Bay of Biscay, for instance, Pingree & New (1989, 1991) report observations of a tidal wave beam with amplitudes ranging from approximately 150 m near the shelf break to 100 m further out into the deep ocean.

In the two-fluid configuration considered here, apart from internal waves propagating in the lower fluid with frequencies less than the buoyancy (Brunt–Väisälä) frequency, it is also possible to have interfacial waves; these, however, propagate without leaking energy into the lower fluid only for frequencies above the Brunt–Väisälä frequency. As a result, ignoring nonlinear effects, interfacial disturbances owing to a tidal wave beam incident and reflected at the interface, would be attenuated far from the region of forcing. This suggests that solitary waves could arise from the interaction of a beam with the thermocline only if radiation damping is relatively light, thus allowing nonlinear steepening to come into play.

In our model, taking the upper fluid layer to be thin relative to the interfacial horizontal length scale, as is typically the case for the upper well-mixed layer of the ocean, light radiation damping results when the thermocline (the strength of which is controlled by the density jump at the interface) is not very weak. Under this condition, nonlinear-steepening and dispersive effects can be brought into balance with radiation damping, and the far-field evolution of the interfacial disturbance induced by a finite-amplitude wave beam is governed by an integral–differential equation of the type derived in Maslowe & Redekopp (1980) and Romanova (1981).

This evolution equation is subject to forcing from the incident and reflected tidal wave beam. The induced disturbance, which propagates to the right of the region where the incident beam hits the thermocline, is a sinusoidal wave with the same frequency as the forcing and wavelength determined by the interfacial long-wave speed, that in turn is controlled by the thermocline strength. The amplitude of this near-field response is a key factor in deciding whether nonlinear steepening is strong enough for solitary waves to form in the far field. Fixing the incident beam, it turns out that the near-field response amplitude becomes small in the limit of a strong or weak thermocline; as a result, no solitary-wave generation is feasible in either of these two extremes, explaining the conclusion reached by Gerkema (2001) that solitary waves arise only when the thermocline is moderately strong.

It appears that the nonlinear long-wave model proposed here could be generalized to account for the Earth's rotation, which is known to modify the propagation direction of tidal wave beams and also to introduce additional dispersive effects in the propagation of disturbances along the thermocline. We shall return to this issue at the end of the paper.

2. Flow model and linear response

Our analysis is based on an inviscid two-fluid configuration sketched in figure 1. A homogeneous fluid of depth h ($0 < z < h$), representing the upper well-mixed layer of the ocean, is bounded by a rigid lid and lies on top of an infinitely deep fluid ($-\infty < z < 0$) which, for simplicity, is taken to be uniformly stratified with (constant) Brunt–Väisälä frequency N_0, and the Boussinesq approximation is made. Denoting the reference density in the lower fluid by ρ_0 and the constant density of the upper layer by $\rho_0(1-\Delta)$, the density jump $\rho_0\Delta$ ($\Delta \ll 1$) across the interface $z = 0$ represents the thermocline.

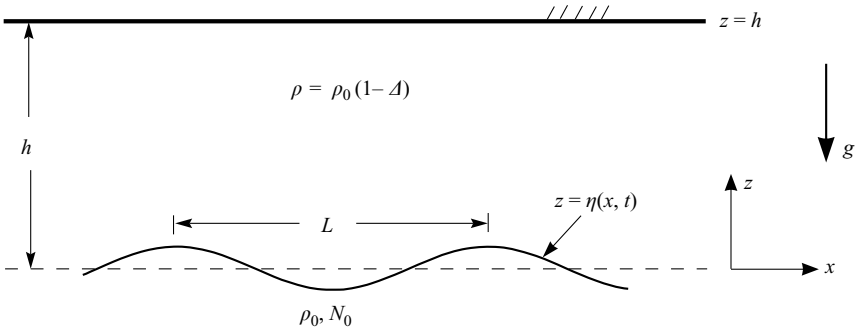

FIGURE 1. Sketch of the two-fluid configuration. The upper fluid layer is homogeneous with density $\rho = \rho_0(1 - \Delta)$. The lower fluid is uniformly stratified and Boussinesq with reference density ρ_0 and constant buoyancy frequency N_0.

This two-fluid system supports interfacial gravity waves owing to the density jump at $z = 0$ as well as internal gravity waves owing to the buoyancy force in the lower fluid; the former are akin to trapped waves propagating along the ocean thermocline, whereas the latter can form wave beams similar to those induced by tidal flow over bottom topography. Our interest centres on the possible generation of interfacial solitary waves by an internal wave beam that is incident and reflected at the interface. To address this issue, we shall study the reflection of a finite-amplitude beam at the interface and the subsequent evolution of the resulting interfacial disturbance.

We begin by summarizing the salient features of the linear response; while nonlinear wave steepening is necessary for the formation of solitary waves, the linear response provides motivation for the appropriate scaling of the nonlinear problem in §3. In dimensionless variables, using h as length scale and h/c_0 as time scale, $c_0 = \left(gh\Delta\right)^{1/2}$ being the long-interfacial-wave speed, the governing equations for linear disturbances consist of Laplace's equation

$$\phi_{xx} + \phi_{zz} = 0 \quad (0 < z < 1), \tag{2.1}$$

for the velocity potential $\phi(x, z, t)$ in the upper fluid layer, and

$$(\zeta_{xx} + \zeta_{zz})_{tt} + \mu^2 \zeta_{xx} = 0 \quad (-\infty < z < 0), \tag{2.2}$$

for the vertical particle displacement $\zeta(x, z, t)$ in the lower fluid, where

$$\mu = \frac{N_0 h}{c_0}. \tag{2.3}$$

These equations are subject to the boundary condition

$$\phi_z = 0 \quad (z = 1) \tag{2.4}$$

at the rigid lid, and the kinematic

$$\eta_t = \phi_z = \zeta_t \quad (z = 0), \tag{2.5}$$

and dynamic

$$\eta_{xx} - \phi_{txx} - \zeta_{ztt} = 0 \quad (z = 0) \tag{2.6}$$

conditions at the interface.

It is clear from (2.2) that harmonic plane waves, $\zeta = f(z)\exp\{\mathrm{i}(kx - \omega t)\}$, propagating along x but confined close to the interface, $f(z) \to 0$ as $z \to -\infty$,

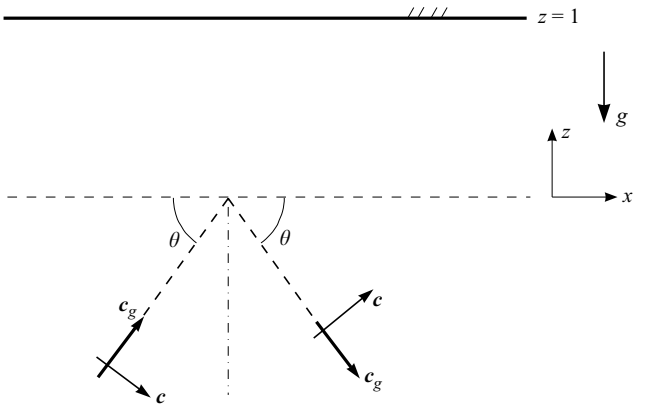

FIGURE 2. A propagating harmonic plane internal wave incident from the lower fluid on the interface at an angle θ to the horizontal and reflected there. The group velocity $\boldsymbol{c}_g$ of the incoming wave points towards the interface, while that of the reflected wave points in the opposite direction. The phase speed $\boldsymbol{c}$ is perpendicular to $\boldsymbol{c}_g$.

can be found only if

$$\omega > \mu. \tag{2.7}$$

This condition is also brought out by the dispersion relation of interfacial waves,

$$\omega^2 = \frac{k \tanh k}{1 + (1 - \mu^2/\omega^2)^{1/2} \tanh |k|}, \tag{2.8}$$

that can be readily obtained from the equation system (2.1)–(2.6), taking $\zeta \to 0$ as $z \to -\infty$. According to (2.8), μ is a cutoff frequency below which k is complex, implying that interfacial waves are evanescent rather than propagating along x when $\omega < \mu$.

According to the field observations (New & Pingree 1990), interfacial disturbances are long compared to h so $k \ll 1$; in this limit, (2.8) can be approximated as

$$\omega^2 = k^2 \left\{1 - (1 - \mu^2/\omega^2)^{1/2}|k| + \cdots\right\}. \tag{2.9}$$

Note that, since $\omega^2 \sim k^2 \ll 1$, $\omega^2 \ll \mu^2$ in general; long interfacial waves, therefore, are strongly evanescent owing to radiation damping unless

$$k \sim \mu \ll 1. \tag{2.10}$$

From the definition of μ in (2.3), it is clear that the condition $\mu \ll 1$, under which long waves propagate subject to light radiation damping along the interface, would not be satisfied if the thermocline happens to be very weak. Since, as will be seen later, nonlinear steepening is possible only under light radiation damping, solitary waves would not be expected to form in the limit of a very weak thermocline.

Consider next a propagating harmonic plane internal wave in the lower fluid incident on the interface at an angle θ to the horizontal (figure 2). The appropriate expressions for ζ, η and ϕ are

$$\zeta = \exp\{\mathrm{i}(kx - lz - \omega t)\} + B \exp\{\mathrm{i}(kx + lz - \omega t)\}, \tag{2.11}$$

$$\eta = A \exp\{\mathrm{i}(kx - \omega t)\}, \tag{2.12}$$

$$\phi = D \cosh k(z - 1) \exp\{\mathrm{i}(kx - \omega t)\}, \tag{2.13}$$

where $k, l > 0$ and $\omega = \mu \sin\theta = \mu k/(k^2 + l^2)^{1/2}$ according to the familiar dispersion relation of internal waves. Note that, in keeping with causality, the wavevectors in (2.12) have been chosen such that the group velocity (and hence the direction of energy transport) associated with the incoming wave points towards the interface, while that of the reflected wave points in the opposite direction.

The undetermined coefficients A, B and D in (2.12)–(2.13) are found by imposing the interfacial conditions (2.5) and (2.6). The reflection coefficient, in particular, satisfies $|B|^2 = 1$ and is consistent with the expression of Delisi & Orlanski (1975) in the short-wave limit ($k \gg 1$). Of more interest here is A, the amplitude of the induced interfacial wave, which in the long-wave limit ($k \ll 1$) can be approximated as

$$A = -\mathrm{i}\,\frac{k\mu^2 \sin 2\theta}{k^2 - \mu^2 \sin^2\theta - \frac{1}{2}\mathrm{i}k\mu^2 \sin 2\theta}. \tag{2.14}$$

As expected, when $\mu \ll 1$ so condition (2.10) is satisfied, the poles of A are close to the real k-axis, corresponding to slightly evanescent interfacial waves.

The interfacial disturbance induced by the reflection of an internal wave beam, incident on the interface at an angle θ to the horizontal, can be readily found by superposition. Specifically, an incoming beam with frequency $\omega = \mu \sin\theta$ takes the form

$$\zeta_{inc} = \frac{\mathrm{e}^{-\mathrm{i}\omega t}}{2\pi} \int_0^\infty Q(k) \exp\{\mathrm{i}k(x - z\cot\theta)\}\,\mathrm{d}k, \tag{2.15}$$

where $Q(k)$ is related to the specific beam profile and k is restricted to $k > 0$, so that energy is transported towards the interface in accordance with figure 2. The induced interfacial disturbance then is

$$\eta = \frac{e^{\mathrm{i}\omega t}}{2\pi} \int_0^\infty Q(k)A(k)e^{\mathrm{i}kx}\,\mathrm{d}k, \tag{2.16}$$

where $A(k)$ is the known interfacial amplitude for plane-wave reflection, given by (2.14) in the long-wave limit.

Since the poles of $A(k)$ are away from the real k-axis, the linear response (2.16) is locally confined, $\eta \to 0$ as $x \to \pm\infty$. However, as remarked earlier, in the case $\mu \ll 1$, A has a pole at $k = k_*$ slightly above the positive k-axis:

$$k_* = \omega + \tfrac{1}{2}\mathrm{i}\omega\mu\cos\theta, \tag{2.17}$$

and this pole provides the far-field response for $x \to \infty$:

$$\eta \sim \frac{\mu^2 \sin 2\theta}{2}\, Q(\omega)\, \exp\left(-\omega\mu\cos\theta\,\frac{x}{2}\right) \mathrm{e}^{\mathrm{i}\omega(x-t)} \qquad (x \to \infty). \tag{2.18}$$

According to (2.18), under flow conditions for which $\mu \ll 1$, the far-field response at the interface propagates to the right of the incident beam only, and is in the form of a long sinusoidal wave with slowly decaying amplitude owing to leaking of energy into the lower fluid. The possibility that nonlinear steepening may overcome the radiation damping of the linear response (2.18) to give rise to solitary waves is examined below.

3. Nonlinear response

3.1. *Reflection of tidal wave beam*

Based on the linear analysis of § 2, long interfacial waves of wavenumber k and frequency ω are subject to light radiation damping, so nonlinear steepening is likely

to be more effective, when $k \sim \omega \sim \mu \ll 1$. This suggests treating μ as a small parameter and re-scaling x and t as follows:

$$X = \mu x, \quad T = \mu t \quad (\mu \ll 1). \tag{3.1}$$

Furthermore, from (2.18), such lightly damped interfacial waves are triggered by wave beams incident on the interface from below at an angle θ to the horizontal, where $\theta = O(1)$ in general. In the lower fluid, therefore, the vertical coordinate is scaled in sympathy with X:

$$Z = \mu z. \tag{3.2}$$

The vertical particle displacement $\zeta(X, Z, T)$ then is governed, to leading order in μ, by a linear equation analogous to (2.2):

$$(\zeta_{XX} + \zeta_{ZZ})_{TT} + \zeta_{XX} = 0 \quad (-\infty < z < \eta), \tag{3.3}$$

even for finite-amplitude disturbances.

Turning next to the interfacial elevation $\eta(X, T)$, according to (2.14), for long waves with $k = O(\mu)$, the ratio of the interfacial amplitude to the incident-wave amplitude is $O(\mu)$. This suggests that the interfacial disturbance induced by a finite-amplitude long-wave beam is weakly nonlinear, namely

$$\eta = \mu\tilde{\eta}; \tag{3.4}$$

as a result, to leading order in μ, the linearized interfacial conditions (2.5) and (2.6) on $z = 0$ continue to hold:

$$\phi_z = \mu\zeta_T = \mu^2\tilde{\eta}_T \quad (z = 0), \tag{3.5}$$

$$\tilde{\eta}_{XX} - \phi_{TXX} - \zeta_{ZTT} = 0 \qquad (z = 0). \tag{3.6}$$

Furthermore, the velocity potential in the upper fluid layer, $\phi(z; X, T)$, which satisfies Laplace's equation (2.1) and the rigid-lid condition (2.4), can be expanded as

$$\phi = a(X, T) - \tfrac{1}{2}\mu^2(z-1)^2 a_{XX} + \cdots. \tag{3.7}$$

Therefore, according to (3.5), $\tilde{\eta}_T = a_{XX} = \phi_{XX}$ so (3.6) becomes a forced wave equation for $\tilde{\eta}(X, T)$:

$$\tilde{\eta}_{XX} - \tilde{\eta}_{TT} = \zeta_{ZTT}|_{Z=0}. \tag{3.8}$$

The forcing on the right-hand side of (3.8) derives from the incident and reflected internal wave beam at the interface. Specifically, for a finite-amplitude beam incident at an angle θ to the horizontal with frequency $\Omega = \sin\theta$, it follows from (3.3) that

$$\zeta = \{q(X - Z\cot\theta) + r(X + Z\cot\theta)\}\,\mathrm{e}^{-\mathrm{i}\Omega T} + \text{c.c.}, \tag{3.9}$$

where c.c. stands for the complex conjugate. However, according to (3.5), $\zeta = O(\mu)$ on $Z = 0$, implying that the incident beam is nearly perfectly reflected at the interface, so $r(X) = -q(X)$ to leading order. Hence,

$$\zeta_{ZTT}|_{Z=0} = 2\Omega^2\cot\theta\, q_X\,\mathrm{e}^{-\mathrm{i}\Omega T} + \text{c.c.}, \tag{3.10}$$

where

$$q(X) = \frac{1}{2\pi}\int_0^\infty \hat{q}(k)\,\mathrm{e}^{\mathrm{i}kX}\,\mathrm{d}k, \tag{3.11}$$

in accordance with the radiation condition noted earlier (see figure 2), requiring the incoming and reflected beam profiles $q(X)$ and $r(X)$ to involve plane waves with $k > 0$ only.

Finally, inserting (3.10) into (3.8), the interfacial response $\tilde{\eta}(X, T)$ satisfies

$$\tilde{\eta}_{XX} - \tilde{\eta}_{TT} = \sin 2\theta \, q_X \, \mathrm{e}^{-\mathrm{i}\Omega T} + \text{c.c.} \tag{3.12}$$

This forced wave equation can be readily solved by taking Fourier transform in X. The response propagates to the right of the incident beam ($X > 0$) only and, assuming that the forcing owing to the incident and reflected beam is turned on at $T = 0$, is given by

$$\tilde{\eta}(X, T) \sim \tfrac{1}{2} \sin 2\theta \, \hat{q}(\Omega) \, \mathrm{e}^{\mathrm{i}\Omega(X-T)} \mathrm{H}(T - X) + \text{c.c.} \quad (X \to \infty), \tag{3.13}$$

where $\mathrm{H}(X)$ stands for the Heaviside function. According to (3.13), to leading order in μ, the reflection of a finite-amplitude beam at the interface gives rise to a weakly nonlinear sinusoidal long wave there, which propagates to the right of the incident beam.

The wave amplitude in (3.13), being proportional to $\hat{q}(\Omega)$, depends on the incoming-beam profile. To bring out this effect more clearly, it is convenient to introduce the parameter

$$\alpha = \frac{N_0 L}{c_0}, \tag{3.14}$$

where L denotes the characteristic beam width. Note that α measures the width along the interface of the incoming-beam profile, $L/\sin\theta$, in comparison to $2\pi c_0/(N_0 \sin\theta)$, the wavelength of the generated long wave (3.13) on the interface. In terms of α, the incident beam then takes the form

$$\zeta_{\text{inc}} = F(\chi/\alpha) \, \mathrm{e}^{-\mathrm{i}\Omega T} + \text{c.c.} \tag{3.15}$$

with

$$F(\chi/\alpha) = \frac{1}{2\pi} \int_0^\infty \mathrm{e}^{\mathrm{i}k\chi/\alpha} \, \hat{F}(k) \, \mathrm{d}k, \tag{3.16}$$

where $\chi = X \sin\theta - Z \cos\theta$ is the cross-beam coordinate and, in view of (3.9),

$$q(X) = F(X \sin\theta/\alpha). \tag{3.17}$$

Therefore, since $\Omega = \sin\theta$,

$$\hat{q}(\Omega) = \frac{\alpha}{\sin\theta} \hat{F}(\alpha), \tag{3.18}$$

and (3.13) becomes

$$\tilde{\eta}(X, T) \sim \alpha \hat{F}(\alpha) \cos\theta \, \mathrm{e}^{\mathrm{i}\Omega(X-T)} \mathrm{H}(T - X) + \text{c.c.} \quad (X \to \infty). \tag{3.19}$$

From (3.19), it is now clear that the amplitude of the induced interfacial wave, which is a major control of the nonlinear steepening, hinges on the value of the parameter α. In particular, fixing the beam profile and angle of incidence, the maximum wave amplitude on the interface is expected when $\alpha = O(1)$; as discussed later (see §4), this flow regime is realized when the thermocline is of moderate strength.

We also remark that, unlike the linear interfacial response (2.18) obtained earlier, expressions (3.13) and (3.19) do not include radiation damping; this comes into play for $X = O(1/\mu)$ along with the nonlinear and dispersive effects. A far-field analysis that takes into account these effects is presented below.

3.2. *Far-field evolution*

For the purpose of analysing the far-field response, we shall adopt a reference frame moving with the interfacial linear-long-wave speed, $\Theta = X - T$, and introduce

$\xi = \mu X = \mu^2 x$ so that $\xi = O(1)$ in the far field. In terms of these variables, the near-field response (3.19) may be viewed as an 'inner' solution valid as $\xi \to 0$, and the far-field response $\tilde{\eta}(\Theta, \xi)$ $(-\infty < \Theta < \infty,\ \xi > 0)$, which is the 'outer' solution, obeys the matching condition:

$$\tilde{\eta} \to \alpha \hat{F}(\alpha) \cos\theta \, \mathrm{e}^{\mathrm{i}\Omega\Theta} \mathrm{H}(-\Theta) + \text{c.c.} \quad (\xi \to 0). \tag{3.20}$$

As the incident and reflected beam is not present in the far field, $\tilde{\eta}(\Theta, \xi)$ thus propagates as a free disturbance for $\xi > 0$, and (3.20) provides the necessary connection with the forcing owing to these beams.

We now derive an equation that governs the evolution of the far-field response for $\xi > 0$. Consider the lower fluid first. Since no forcing is present, the far-field vertical particle displacement accompanying $\tilde{\eta}(\Theta, \xi)$ is weakly nonlinear, $\zeta = \mu\tilde{\zeta}(\Theta, Z, \xi)$ and, from (3.3), satisfies the linear equation

$$\tilde{\zeta}_{\Theta\Theta} + \tilde{\zeta}_{ZZ} + \tilde{\zeta} = 0 \quad (-\infty < Z < 0), \tag{3.21}$$

to leading order in μ.

Turning next to the upper fluid layer, using Laplace's equation (2.1) along with the rigid-lid condition (2.4), the velocity potential $\phi(z; \Theta, \xi)$ has an expansion analogous to (3.7):

$$\phi = \tilde{a}(\Theta, \xi) - \tfrac{1}{2}\mu^2(z-1)^2\tilde{a}_{\Theta\Theta} - \mu^3(z-1)^2\tilde{a}_{\Theta\xi} + \cdots. \tag{3.22}$$

Imposing the kinematic conditions at the interface $z = \mu\tilde{\eta}$ and making use of (3.22) then yields

$$\tilde{a}_\Theta = -\tilde{\eta} - \mu\tilde{\eta}^2 - 2\mu\tilde{a}_\xi + O(\mu^2), \tag{3.23}$$

$$\tilde{\zeta}|_{Z=0} = \tilde{\eta} + O(\mu^2). \tag{3.24}$$

Finally, the dynamic condition requires the pressure to be continuous at the interface $z = \mu\tilde{\eta}$. For our two-fluid system, Thorpe (1998) has derived an approximation to this condition, correct to second order in the amplitude, that can be applied at $z = 0$. Implementing the long-wave scalings valid here, this leads to

$$(\tilde{\eta} + \tilde{a}_\Theta)_\Theta + \mu\left(\tilde{\eta}_\xi + \tilde{a}_{\Theta\xi} - \tfrac{1}{2}(\tilde{a}_\Theta^2)_\Theta - \tilde{\zeta}_{\Theta Z}|_{Z=0}\right) = O(\mu^2). \tag{3.25}$$

Using then (3.23) to eliminate $\tilde{a}$ from (3.25) results in the following evolution equation for $\tilde{\eta}(\Theta, \xi)$:

$$2\tilde{\eta}_\xi - 3\tilde{\eta}\tilde{\eta}_\Theta - (\tilde{\zeta}_Z|_{Z=0})_\Theta = 0. \tag{3.26}$$

The third term in (3.26), which accounts for the presence of the lower fluid, can be expressed in terms of $\tilde{\eta}$ by solving (3.21) subject to the boundary condition (3.24) on $Z = 0$ and the appropriate radiation condition as $Z \to -\infty$. Specifically, taking the Fourier transform in Θ,

$$\hat{\eta}(\kappa; \xi) = \int_{-\infty}^{\infty} \mathrm{e}^{-\mathrm{i}\kappa\Theta} \, \tilde{\eta}(\Theta, \xi) \, \mathrm{d}\Theta, \tag{3.27}$$

we have

$$\tilde{\zeta}_Z|_{Z=0} = \frac{1}{2\pi} \int_{-\infty}^{\infty} \mathrm{i}\, m \, \mathrm{e}^{\mathrm{i}\kappa\Theta} \, \hat{\eta}(\kappa; \xi) \, \mathrm{d}\kappa, \tag{3.28}$$

where

$$m = \begin{cases} -\mathrm{i}\,(\kappa^2 - 1)^{1/2} & (\kappa^2 > 1), \\ \mathrm{sgn}\kappa\,(1 - \kappa^2)^{1/2} & (\kappa^2 < 1). \end{cases} \tag{3.29}$$

The choice of the branch of the square root in (3.29) is dictated by causality; it ensures that, as $Z \to -\infty$, the disturbance in the lower fluid either decays (for $\kappa^2 > 1$) or transports energy away from the interface (for $\kappa^2 < 1$), resulting in radiation damping of $\tilde{\eta}$.

Combining (3.26) with (3.28), the evolution equation governing the far-field response $\tilde{\eta}(\Theta, \xi)$,

$$2\tilde{\eta}_\xi - 3\tilde{\eta}\tilde{\eta}_\Theta + \frac{1}{2\pi}\int_{-\infty}^{\infty} \kappa\, m\, \mathrm{e}^{\mathrm{i}\kappa\Theta}\, \hat{\eta}(\kappa;\xi)\, \mathrm{d}\kappa = 0, \tag{3.30}$$

is an integral–differential equation of the type derived earlier by Maslowe & Redekopp (1980) for the purpose of discussing the radiation damping of weakly nonlinear long waves in stratified shear flows of large depth. The same equation was also obtained independently by Romanova (1981). If the lower fluid is not stratified so radiation damping is absent, (3.29) is replaced by $m = -\mathrm{i}|\kappa|$ and (3.30) reduces to the familiar Benjamin–Davis–Ono (BDO) equation for the propagation of long interfacial waves in deep fluids. As is well known, the BDO equation admits solitary-wave solutions with algebraic profiles.

In the present context, (3.30) is to be solved subject to the 'initial' condition (3.20) at $\xi = 0$ that ensures matching with the near-field response. Ignoring nonlinearity, the far-field response eventually decays via radiation damping as implied by (2.18), and the question of interest here is whether nonlinear steepening, represented by the second term in (3.30), can reverse this trend so that the disturbance induced by the tidal beam can give rise to solitary waves. This issue is now taken up by solving (3.30) subject to (3.20) numerically.

4. Numerical results

In our computations, the incident tidal beam is taken to have an exponential profile so that

$$\zeta_{inc} = C\exp(-|\chi|/\alpha) \quad (T = 0), \tag{4.1}$$

C being a parameter that controls the peak amplitude of the vertical particle displacement ζ_{inc} associated with the wave beam. The choice (4.1) corresponds to

$$\hat{F}(k) = \frac{2C}{1+k^2} \tag{4.2}$$

in (3.16).

The evolution equation (3.30) for $\tilde{\eta}(\Theta, \xi)$ is solved numerically as an initial-value problem, treating the matching condition (3.20) as initial condition at $\xi = 0$ and advancing $\tilde{\eta}$ in $\xi > 0$. For this purpose, we employ a pseudospectral technique in which, at each step $\Delta\xi$, the nonlinear term in (3.30) is advanced by a forward Euler finite-difference scheme while the linear term is treated by Fourier transform using the fast Fourier transform in a finite computational domain $\Theta_{-\infty} < \Theta < \Theta_{+\infty}$.

Using (4.2) in (3.20), the initial condition applied at $\xi = 0$ is

$$\tilde{\eta}(\Theta, \xi = 0) = \frac{4\alpha C\cos\theta}{(1+\alpha^2)}\sin(\Omega\Theta)\mathrm{H}(-\Theta), \tag{4.3}$$

where the phase of the incident wave beam has been chosen so as to avoid a discontinuity at $\Theta = 0$. Moreover, in implementing (4.3) numerically, $\tilde{\eta}(\Theta, \xi = 0)$ was tapered off as $\Theta \to -\infty$ so that the disturbance goes to zero and does not reach the boundaries of the computational domain. Note that although the parameter μ does

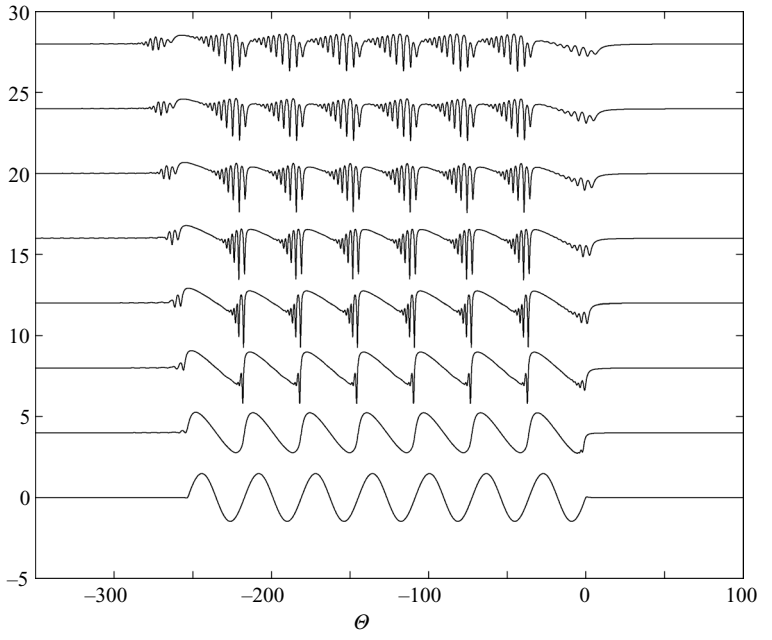

FIGURE 3. The far-field response $\tilde{\eta}(\Theta, \xi)$ at various stations ξ along the interface for the choice of parameters $\theta = 10^\circ$, $C = 0.75$ and $\alpha = 1.0$. The bottom plot is the 'initial' condition (4.3) at $\xi = 0$, and ξ increases upwards by steps of 2.

not affect $\tilde{\eta}(\Theta, \xi)$, it plays an important part in transforming the spatial evolution $\tilde{\eta}(\Theta, \xi)$ to the temporal evolution $\tilde{\eta}(X, T)$, as well as in determining the interface elevation, $\eta = \mu\tilde{\eta}$.

Figure 3 displays results at different values of ξ from a sample run using a computational domain $\Theta_{+\infty} - \Theta_{-\infty} = 1536$ with 8192 grid points along Θ and step size $\Delta\xi = 0.0001$, for the choice of parameters $\theta = 10^\circ$, $C = 0.75$ and $\alpha = 1.0$. Each station ξ specifies a fixed location along the interface, and $\tilde{\eta}(\Theta, \xi)$ furnishes the corresponding time history of the response there. The sinusoidal disturbance triggered by the beam initially steepens in a typical hyperbolic fashion owing to the nonlinear term in (3.30) and, as dispersive effects become important, trains of solitary waves are seen to emerge, but eventually radiation damping comes into play, causing the solitary waves to decay far from the region of forcing.

We now apply our model to the local generation of solitary waves in the ocean thermocline. For the tidal period $\tau = 12\,\text{h}$, the angle θ at which the incoming beam hits the thermocline is fixed by the dispersion relation of internal waves in the lower fluid, $\sin\theta = \tau/(2\pi N_0)$. In the ocean, the buoyancy frequency N_0 is in the range $1\text{–}3 \times 10^{-3}\,\text{s}^{-1}$, so θ varies between roughly 3° and 8°. Moreover, taking $h = 60\,\text{m}$ and $\Delta = 1.5 \times 10^{-3}$ as in Gerkema (2001), it follows from (2.3) that the parameter μ is in the range $0.06 - 0.2$. We chose $N_0 = 2 \times 10^{-3}\,\text{s}^{-1}$, the value of N_0 assumed by Gerkema (2001), which implies $\theta = 4.17^\circ$ and $\mu = 0.128$. We also took $\alpha = 0.65$, corresponding to an incoming beam of width roughly 25 km along the horizontal, as suggested by figure 3 of Gerkema (2001). Finally, we used a computational domain $\Theta_{+\infty} - \Theta_{-\infty} = 2048$ with 8192 points along Θ and step size $\Delta\xi = 0.0001$.

Figure 4 shows snapshots every 1.5 h within a tidal period of the interface elevation η in dimensional variables for three values of the amplitude parameter, $C = 0.75$,

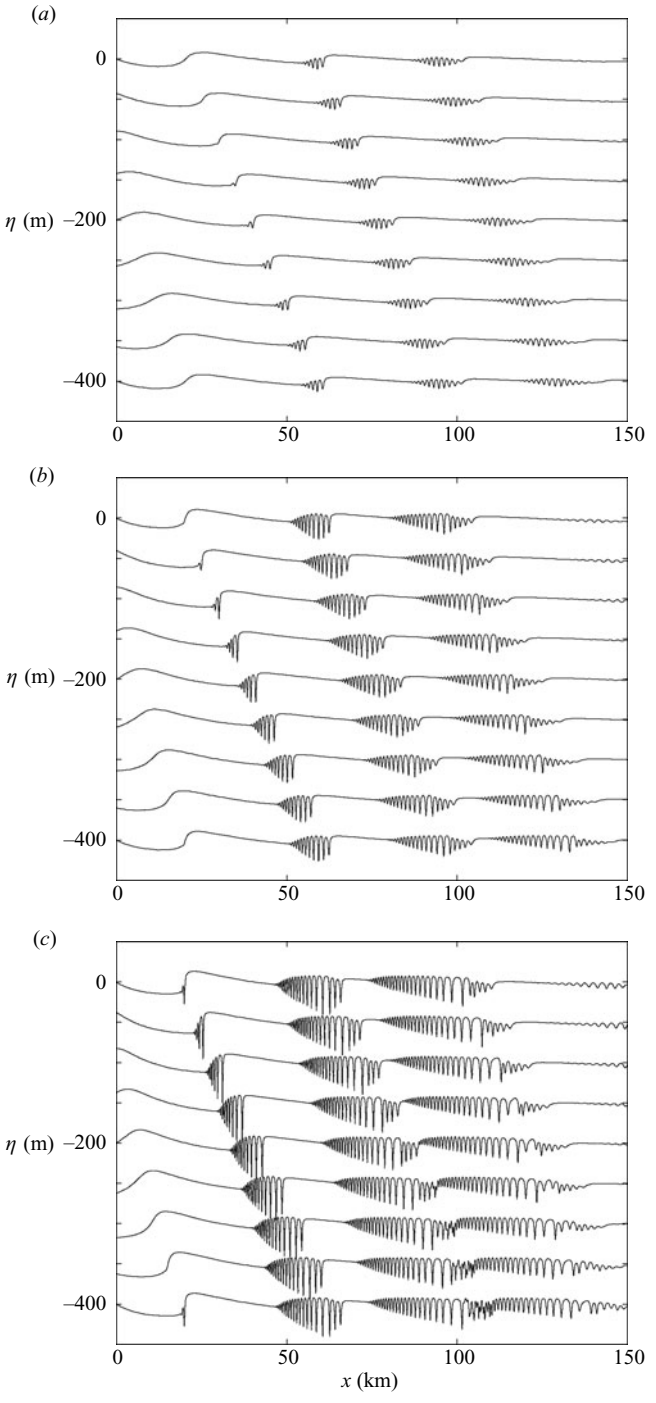

FIGURE 4. Snapshots of the far-field interfacial response induced by a tidal beam incident on the thermocline at an angle $\theta = 4.17^\circ$ to the horizontal, under flow conditions corresponding to $\mu = 0.128$. The interface elevation η is displayed every 1.5 h within a tidal period, 42 h after the beam has been turned on (time increases from top to bottom). The beam profile has fixed width, corresponding to $\alpha = 0.65$ in (4.1), and the amplitude parameter C is varied: (*a*) $C = 0.75$; (*b*) $C = 1.0$; (*c*) $C = 1.25$.

$C = 1.0$ and $C = 1.25$, that correspond, respectively, to peak vertical-displacement amplitudes of 45 m, 60 m and 75 m for the incoming beam. Clearly, the generation mechanism of solitary waves is sensitive to the beam strength; increasing the amplitude of the incoming beam from 45 m to 75 m causes the generated solitary waves to be significantly steeper and to form closer to the region where the beam reflects at the thermocline. While no direct comparison can be made with the simulations in Gerkema (2001), the evolution depicted in figure 4(*b*) for a beam with peak amplitude 60 m is similar to the evolution of the interface shown in his figure 8 for a moderate-strength thermocline. Note, in particular, that solitary waves first appear on a trough of the induced disturbance, roughly 35 km from the position where the beam impacts the thermocline, attain a peak amplitude of about 25 m and then gradually decay owing to radiation damping, in qualitative agreement with Gerkema's simulation.

We next turn to the role of the thermocline strength in the local generation of solitary waves. In the present two-layer flow configuration, the strength of the thermocline is controlled by the density jump Δ at the interface, which affects the long-wave speed c_0 and thereby the values of the flow parameters μ and α defined in (2.3) and (3.14), respectively; in particular, if Δ is increased (decreased), the rest of the flow and the beam specifications being fixed, the parameters μ and α decrease (increase). In the course of varying Δ, however, since $\alpha \hat{f}(\alpha) \to 0$ for $\alpha \ll 1$ and $\alpha \gg 1$, the amplitude of the near-field response (4.3) is expected to attain a maximum value when $\alpha = O(1)$, indicating that the optimal condition for solitary waves to be generated in the far field would result when the thermocline is of moderate strength.

Figure 5 shows the effect of varying Δ on the values of the parameters α, μ and the amplitude of the near-field response (4.3) under the flow conditions chosen earlier and for the same incident beam as in figure 4(*b*). Note that the maximum amplitude is obtained for $\alpha = 1.0$ ($\Delta = 0.63 \times 10^{-3}$), while the response shown in figure 4(*b*) corresponds to a stronger thermocline ($\alpha = 0.65$, $\Delta = 1.5 \times 10^{-3}$) than the optimal. This indicates that appreciable solitary waves can be generated for a range of intermediate thermocline strengths. Of course, as the amplitude of the near-field response (4.3) is proportional to C, the range of thermocline strengths for which local generation of solitary waves is feasible, depends on the peak amplitude of the incident wave beam.

Outside this range, the amplitude of the near-field response (4.3) is small so nonlinear steepening is relatively insignificant and no appreciable solitary waves arise, as illustrated in figure 6. In the case of a strong thermocline, in particular, the interface is disturbed very little (figure 6*a*) while, in the other extreme of a very weak thermocline, the response is dominated by radiation damping, with only small-amplitude wavetrains propagating in the far field (figure 6*b*). These computations were carried out using the same resolution as those in figure 4, and the results are in qualitative agreement with the numerical simulations in figure 8 of Gerkema (2001).

5. Discussion

We have developed a nonlinear long-wave theory for the interaction of an internal tidal wave beam with the ocean thermocline and for the ensuing local generation of solitary waves in the context of a two-layer flow configuration, representing the thermocline as a density jump across the interface between a homogeneous upper layer and an infinitely deep uniformly stratified fluid. Apart from providing theoretical confirmation of the two-stage process envisaged by Gerkema (2001), the proposed asymptotic model enables us to examine systematically the conditions under which

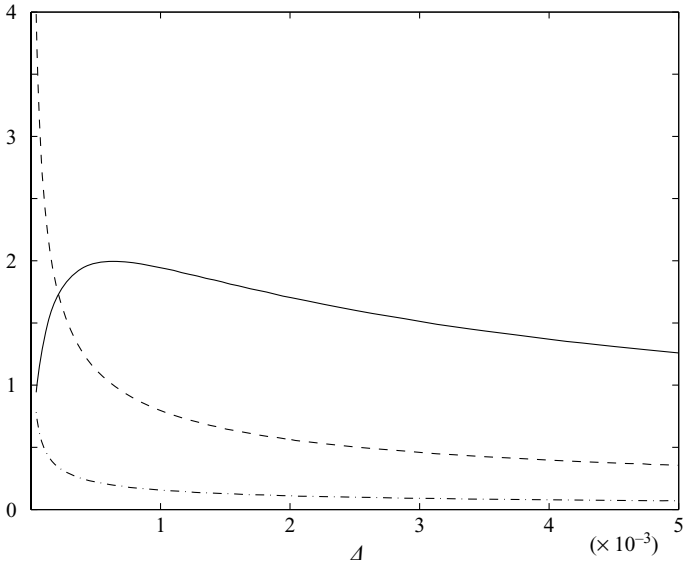

FIGURE 5. Variation with the thermocline strength Δ of the flow parameters μ (—·—), α (— — —) and the amplitude of the 'initial' condition (4.3), $4\alpha C\cos\theta/(1+\alpha^2)$ (—).

solitary waves can arise and reveals several useful insights into the local generation mechanism.

The evolution of the induced wave disturbance in the thermocline depends primarily on the parameters μ and α defined in (2.3) and (3.14), respectively, as well as on the beam peak-amplitude parameter C; the angle of incidence θ of the wave beam is fixed by the tidal frequency, given the buoyancy frequency in the lower fluid. The asymptotic theory assumes that $\mu \ll 1$; under this condition, long-wave disturbances in the thermocline are only lightly attenuated owing to leakage of energy into the lower fluid, making it possible for nonlinear steepening and dispersive effects to be brought into balance with radiation damping. In this distinguished limit, the far-field evolution is governed by the integral–differential equation (3.30), a generalization of the BDO equation that accounts for radiation damping. Ultimately, whether or not solitary waves are generated, however, is determined by the amplitude of the response close to the region where the beam hits the thermocline, and the parameters α and C play an important part in this respect.

The optimal setting for solitary-wave generation is realized when $C = O(1)$ and $\alpha = O(1)$, as the amplitude of the near-field response turns out to be maximum under these conditions, thus leading to the strongest nonlinear steepening in the far field. Specifically, for $\mu \ll 1$, the analysis shows that a finite-amplitude ($C = O(1)$) incident wave beam induces a weakly nonlinear ($O(\mu)$) disturbance on the interface, confirming the assertion of Gerkema (2001) that the scattering of the beam at the interface is essentially a linear process. In the vicinity of the region where the beam hits the thermocline, the response is a sinusoidal long wave with the same frequency as the forcing and propagates to the right of the incident beam, in keeping with the radiation conditions obeyed by the incident and reflected beams. The amplitude of this near-field response, as expected, is proportional to C, but it is also controlled by the parameter α, which measures the width of the incoming beam along the interface relative to the wavelength of the propagating wave on the interface. When $\alpha = O(1)$,

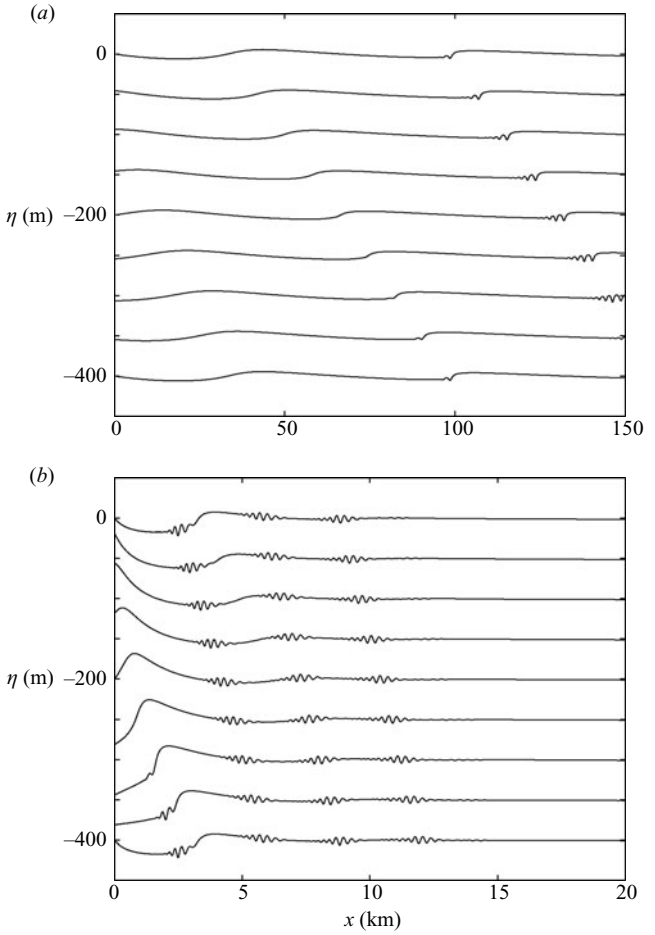

FIGURE 6. Snapshots of the far-field interfacial response induced by a tidal beam incident on the thermocline at an angle $\theta = 4.17^\circ$ to the horizontal. The interface elevation η is displayed every 1.5 h within a tidal period, 42 h after the beam has been turned on (time increases from top to bottom). The beam profile has fixed peak amplitude ($C = 1$) and width. The thermocline strength is varied: (*a*) strong thermocline, $\Delta = 4.0 \times 10^{-3}$ ($\mu = 0.078$, $\alpha = 0.4$); (*b*) weak thermocline, $\Delta = 0.04 \times 10^{-3}$ ($\mu = 0.78$, $\alpha = 4$).

these two length scales are comparable, so the forcing owing to the incident beam is most effective, and the near-field response attains its maximum amplitude.

In the light of these scalings, it is easy to understand the finding of Gerkema (2001) that solitary waves form only when the thermocline is of moderate strength. Indeed, increasing (decreasing) the thermocline strength causes the interfacial long-wave speed c_0 to increase (decrease) as well and, since the forcing frequency is fixed by the tide, this amounts to increasing (decreasing) the wavelength of the induced wave on the interface. Therefore, assuming the incoming-beam profile is held fixed as in Gerkema (2001), increasing (decreasing) the strength of the thermocline is equivalent to decreasing (increasing) the parameter α, the most favourable condition for solitary-wave generation, $\alpha = O(1)$, thus corresponding to an intermediate range of thermocline strengths.

Based on numerical solutions of the far-field evolution equation (3.30) for typical oceanic conditions, the local solitary-wave generation mechanism is quite sensitive to the peak amplitude of the incoming beam, controlled by the parameter C, and increasing C broadens the range of thermocline strengths for which solitary waves arise.

Finally, the present theory ignores the Earth's rotation. The effects of rotation will show up in the propagation of the incoming internal wave beam in the lower fluid as well as in the evolution of the disturbance on the interface owing to the beam reflection. Including rotation in the lower fluid, in particular, the dispersion relation $\omega^2 = \mu^2 \sin^2\theta$ used in our analysis is replaced by

$$\omega^2 = \mu^2 \sin^2\theta + \gamma^2 \cos^2\theta, \tag{5.1}$$

where

$$\gamma = \frac{fh}{c_0}, \tag{5.2}$$

f being the Coriolis parameter. Hence, the angle of incidence θ of the incoming beam is reduced by the rotation, and this effect would be important since the Coriolis parameter typically is comparable to the frequency of the internal tides. For instance, the value $\theta = 4.17^\circ$ obtained earlier for $f = 0$ under the flow conditions used in the computations shown in figure 4, would decrease to $\theta = 3.03^\circ$ for $f = 1.0 \times 10^{-4}\,\mathrm{s}^{-1}$, a value of the Coriolis parameter appropriate in the Bay of Biscay. This, in turn, would cause the vertical-displacement amplitude of the incoming beam, controlled by the parameter C, to decrease by the factor $\sin 3.03^\circ / \sin 4.17^\circ = 0.72$, implying that rotation would inhibit the formation of solitary waves, as noted in Gerkema (2001). We remark, however, that the responses shown in figure 4 are due to beams with relatively low vertical-displacement peak amplitudes; even the largest value of $C = 1.25$ (figure 4*c*) corresponds to 75 m, which is in the very low end of the range of observed beam amplitudes reported by Pingree & New (1989, 1991) in the Bay of Biscay. This suggests that a strong enough incident beam could still generate solitary waves when the effect of the Earth's rotation on the angle of propagation is taken into account.

On the other hand, the Earth's rotation would appear to play a less prominent role in the evolution of the solitary waves, given that these form quite quickly relative to the tidal period according to our results. More specifically, based on a simple *ad hoc* analysis, adding a term γ^2 to the right-hand side of the interfacial dispersion relation (2.9), it is seen that the effect of rotation is measured by the parameter $\gamma^2/\mu^3 = (f/N_0)^2/\mu$ in the long-wave regime (2.10) of interest here. Now, under typical conditions, $f/N_0 \leqslant 0.1$ while μ is in the range $5 \times 10^{-2} - 0.2$, indicating that γ^2/μ^3 in fact is quite small, at most 0.1. This suggests that rotation will not play a significant role in the evolution of the solitary waves, but after a long distance of travel will affect their eventual decay; this scenario could be taken into account by replacing the evolution equation (3.30) with an Ostrovsky-type equation (Grimshaw *et al.* 1998).

We thank Professor Victor Shrira and Dr Theo Gerkema, who read an earlier version of this paper and made several useful suggestions. This work was initiated while T.R.A. was visiting Loughborough University and S.R.C. was visiting University College, London. Both wish to acknowledge the support of EPSRC grants which made these visits possible. T.R.A. also acknowledges the Air Force Office of Scientific Research, Air Force Materials Command, USAF, Grant FA9950-04-1-0125 and the National Science Foundation Grant DMS-0305940.

REFERENCES

Azevedo, A., da Silva, J. C. B. & New, A. L. 2006 On the generation and propagation of internal solitary waves in the southern Bay of Biscay. *Deep-Sea Res.* **53**, 927–941.

Bell, T. H. 1975 Lee waves in stratified flows with simple harmonic time dependence. *J. Fluid Mech.* **67**, 705–722.

Delisi, D. P. & Orlanski, I. 1975 On the role of density jumps in the reflexion and breaking of internal gravity waves. *J. Fluid Mech.* **69**, 445–464.

Gerkema, T. 2001 Internal and interfacial tides: beam scattering and local generation of solitary waves. *J. Mar. Res.* **59**, 227–255.

Grimshaw, R. 2001 Internal solitary waves. *In Environmental Stratified Flows* (ed. R. Grimshaw). Kluwer.

Grimshaw, R. H. J., Ostrovsky, L. A., Shrira, V. I. & Stepanyants, Yu. A. 1998 Long nonlinear surface and internal gravity waves in a rotating ocean. *Nonlinear Processes Geophys.* **19**, 289–338.

Helfrich, K. R. & Melville, W. K. 2006 Long nonlinear internal waves. *Annu. Rev. Fluid Mech.* **38**, 395–425.

Khatiwala, S. 2003 Generation of internal tides in an ocean of finite depth: analytical and numerical calculations. *Deep-Sea Res.* **50**, 3–21.

Lamb, K. G. 2004 Nonlinear interaction among internal wave beams generated by tidal flow over supercritical topography. *Geophys. Res. Lett.* **31**, doi: 10.1029/2003GL019393.

Maslowe, S. A. & Redekopp, L. G. 1980 Long nonlinear waves in stratified shear flows. *J. Fluid Mech.* **101**, 321–348.

New, A. L. & Pingree, R. D. 1990 Large-amplitude internal soliton packets in the central Bay of Biscay. *Deep-Sea Res.* **37**, 513–524.

New, A. L. & Pingree, R. D. 1992 Local generation of internal soliton packets in the central Bay of Biscay. *Deep-Sea Res.* **39**, 1521–1534.

New, A. L. & da Silva, J. C. B. 2002 Remote-sensing evidence for the local generation of internal soliton packets in the central Bay of Biscay. *Deep-Sea Res.* **49**, 915–934.

Pingree, R. D. & New, A. L. 1989 Downward propagation of internal tidal energy into the Bay of Biscay. *Deep-Sea Res.* **36**, 735–758.

Pingree, R. D. & New, A. L. 1991 Abyssal penetration and bottom reflection of internal tidal energy in the Bay of Biscay. *J. Phys. Oceanogr.* **21**, 28–39.

Romanova, N. N. 1981 Generalization of the Benjamin–Ono equation for a weakly stratified atmosphere. *Izv. Atmos. Oceanic Phys.* **17**, 98–101.

Thorpe, S. A. 1998 Nonlinear reflection of internal waves at a density discontinuity at the base of the mixed layer. *J. Phys. Oceanogr.* **28**, 1853–1860.